2D and 3D numerical study of the conjugate radiation and turbulent natural convection heat transfer effect on the cooling process of a HAWT nacelle operating in the Algerian Saharan climate

M. A. Mahdi[a], A. Smaili[a] and Y. Saad[b]

[a]Laboratoire de Génie Mécanique et Développement, Ecole Nationale Polytechnique, El-Harrach, Algiers, 16200, Algeria; [b]Department of Computer Science and Engineering, University of Minnesota, Minneapolis, Minnesota, 55455, USA

ARTICLE HISTORY
Compiled October 9, 2018

ABSTRACT
Nacelles of wind turbines intended to operate under the extreme weather conditions of the Algerian Sahara would be subjected to the overheating problem, especially the electromechanical equipment (e.g. generator, gearbox) becoming less effective as they heat up during use. The present work investigates numerically the impact of conjugate heat transfer by turbulent natural convection and radiation on the thermal behavior of the nacelle. Reynolds-Averaged Navier-Stokes and energy equations have been considered, where ANSYS FLUENT code has been employed to solve the resulting mathematical model. An iterative procedure for mesh and time-step dependency study has been proposed. The resulting fields of temperature and velocity within the nacelle have been presented and discussed both in 2D and 3D-configurations, where detailed numerical validations have been carried out. The impact of convective and radiative heat transfers has been quantified and analyzed inside and outside the nacelle. Effects of the internal and external thermal loads on the cooling power have shown the drastic impact of the Saharan climate on the nacelle thermal behavior.

KEYWORDS
Saharan climate; wind turbine nacelle; numerical simulation; cooling system; nacelle thermal behavior

1. Introduction

The Algerian Sahara is characterized by extremely severe climatic conditions where temperature reaches high levels. Saharan regions usually feature high diurnal temperature variations between days and nights and from one season to another. Moreover, ambient air is usually laden with dust particles. This effect is especially significant in sandy and desert regions where strong winds are able to suspend and transport sand particles at considerable heights (Pechlivanoglou et al., 2010). The Horizontal Axis Wind Turbines (HAWT) intended to operate under such extreme conditions run the risk of failure being subjected to constraints of design and conception difficulties. On the other hand, the electromechanical equipment inside the nacelle such as generator, gearbox, converter and power packs, become less effective as they heat up during

CONTACT M. A. Mahdi. Email: mohammed_amokrane.mahdi@g.enp.edu.dz

use, due to Joule effect and friction. Therefore, keeping these equipment at the right temperature is crucial to get the best performance out of the wind turbine.

For this aim, the nacelle should be air-tight and an active cooling system must be employed to ensure an appropriate temperature of the air inside the nacelle. However, most wind turbine cooling systems have a maximum ambient temperature level above which they cannot operate to ensure sufficient cooling performance in order to maintain the design operational temperature for the different components. This leads to gradual de-rating of the power output and eventually to wind turbine shut-down due to an overheating alarm (Xydis et al., 2015). In order to control properly the resulting heat transfer, a compromise must be determined between the air temperature levels inside the nacelle, and the high cooling efficiency which leads to lower reliability and higher cost for such a complex cooling system.

A numerical method has been developed by Smaili et al. (2006) where the effect of the environment temperature on a wind turbine nacelle operating in the Canadian Nordic climate has been assessed, and the turbine has been modeled using hybrid method. To solve the steady governing equations, Control-Volume Finite Element Method (CVFEM) has been developed. In order to maintain an acceptable temperature level within the nacelle, it has been found that, during summer, the amount of air mass rate flowing through the nacelle should be adjusted properly as function of wind velocity and external temperature. In turn, during winter, the nacelle should be well insulated and the air should be well stirred to obtain nearly uniform temperature distribution within the nacelle. In another work, Smaili et al. (2012), used the same numerical method to investigate the thermal behavior of a 750 kW wind turbine nacelle operating in the Algerian Saharan climate. To simplify the problem, a 2D-configuration has been considered. The effect of gravity was neglected, and air within the nacelle has been assumed to be stationary. Therefore, only heat exchange by steady thermal conduction has been accounted for within the nacelle. Linear trends have been obtained for the required cooling capacity and for the resulting average temperature inside the nacelle with respect to the cooling temperature. It has been found that the environmental heat load constitutes the main contribution (97%) to be balanced by the required cooling capacity during nacelle thermal control.

Recently, a numerical study has been carried out by Mahdi & Smaili (2017a) to investigate the thermal behavior of a hypothetical nacelle operating in hot climate. The aim of this work is to put light on heat exchange by laminar natural convection within the nacelle. For this purpose, the generator and the cooling system have been idealized as isothermal hot and cold plates. On the other hand, in order to stay in the laminar regime range, a scaling factor has been applied on the dimensions of the computational domain. It has been concluded that appropriate values of the required cooling loads are dependent on the accurate predictions of heat transfer by natural convection within the nacelle. In a more recent work Mahdi & Smaili (2017b), more realistic considerations have been taken into account, including the effect of heat transfer by turbulent natural convection and by radiation within the nacelle. A typical commercial wind turbine has been considered, where heat exchange with the surroundings has been modeled using a suitable correlation. Similarly to the prior paper (Smaili et al., 2012), the prominence of the external heat exchange has been also noticed. However, it has been concluded that the heat rate generated within the nacelle constitutes rather a more significant part of the total thermal loads to be balanced by the cooling system. This result tallies with the prior expectations, given the realistic considerations of heat transfer within the nacelle taken into account in this work.

Łapka et al. (2018) have lately published a study on the analysis of engine bay

cooling and ventilation systems as well as heat transfer in the nacelle in a small airplane equipped with a turboprop engine in the tractor arrangement. The 1D and 3D models of complex heat transfer have been compared, where temperature fields on the inner and outer surface of the nacelle for both models have been calculated and discussed.

To our knowledge, no more works on the nacelle thermal behavior have been found in the literature. However, several works on the heat transfer in enclosures with different shapes and configurations have been published. It is of interest to review some of these works since the present study is focusing namely on the same aspect of confined natural convection within enclosures. Here, we center our review particularly on works treating similar aspects to the present study.

Baïri et al. (2014) presented a review of several research works on natural convection in cavities where a large variety of configurations have been investigated (e.g. cavity shape, angle of inclination, convecting fluid nature and radiative properties, thermal boundary conditions). Different approaches, including experimental and numerical methods, have been used to deal with the problem where a wide range of Rayleigh number has been covered to account for turbulence effect. Chiu & Chen (1996) treated the case of transient natural convection heat transfer between concentric and vertical eccentric isothermal spheres. The inner sphere is heated and the outer is cooled. The problem has been approached using the alternating direction implicit method and the successive over-relaxation techniques. The parametric study revealed that the heat and flow fields are primarily dependent on the Rayleigh number and on the vertical eccentricity of the two spheres.

The problem of natural convection in the annulus between horizontal concentric cylinders has been studied by many authors in different configurations. One can cite (Farouk et al., 1982) and (McLeod & Bishop, 1989). The experimental study of the latter investigates the natural convection of helium in the cylindrical annuli at cryogenic temperatures where heat transfer rates and temperature profiles are measured for high values of Rayleigh number varying from 8×10^6 to 2×10^9. Heat transfer data has been correlated in terms of the thermal expansion coefficient and the Rayleigh number based on the cylinders diameters. The effect of turbulence on the convective flow has been reported and discussed.

Many authors in the last decades have been interested by the problem of natural convection combined with surface radiation in enclosures with fins or obstructions in the form of solid bodies. Ma & Xu (2016) treated the problem of unsteady natural convection in a differentially heated cavity with a fin for high Rayleigh numbers from 10^8 to 10^{11} where the transient features of natural convection flows in the cavity have been described. It has been concluded that the development of natural convection from the start-up is dependent on the Rayleigh number and the fin position.

Liu & Phan-Thien (1999) studied the case of conjugate conduction, radiation and natural convection in a vertical square cavity inside of which a solid body is heated. The numerical study has shown that temperature and velocity fields are strongly influenced by radiation effects. Mezrhab et al. (2006) conducted a numerical investigation of the combined radiation and natural convection problem in a differentially heated square cavity with a centered square block. It has been found that the average Nusselt number is proportional to radiation which in turn homogenizes temperature filed in the cavity, in particular when Rayleigh number and solid-fluid thermal conductivity ratio are high. A numerical study on the surface radiation effect on the breakdown of steady natural convection flows in a square cavity with a centered hot isothermal square body has been performed by Sun et al. (2011). It has been shown that Rayleigh number transition value to the unsteady regimes increases strongly under the influence of

radiation. Liao & Lin (2014) studied numerically the transitions of natural convection flows in a square enclosure with a heated circular cylinder using an immersed-boundary method. The influence of Prandtl and Rayleigh numbers on the flow regimes has been investigated.

Several other physical aspects and their impact on confined natural convection problem have been investigated by many authors in the last decades. The problem of thermal stratification in a convecting flow within enclosures is one of the most emphasized, e.g. (Wu & Lei, 2015) and Le Quéré and coworkers: (Sergent et al., 2013a), (Sergent et al., 2013b), (Xin et al., 2013).

This paper presents a numerical method to investigate the impact of conjugate heat exchange by turbulent natural convection and radiation on the nacelle thermal behavior, where both 2D and 3D-configurations are considered. To determine the optimal simulation parameters (grid and time-step size), an iterative procedure has been proposed for mesh and time-step dependency study, where a flowchart diagram has been presented in detail. In order to investigate the validity of the numerical method in the 2D-case, an analysis of the thermal stratification of the air within the nacelle is carried out. On the other hand, the 3D-case results have been validated by comparing the obtained temperature and velocity distributions in the cylindrical annuli part of the nacelle with the benchmark work of McLeod & Bishop (1989). Detailed results including temperature and velocity fields within the nacelle have been presented and thoroughly discussed. The resulting average temperature inside the nacelle as well as the required cooling capacity have been quantified, where interesting conclusions have been drawn concerning the nacelle thermal behavior.

2. Mathematical model

2.1. Physical problem

Figure 1 shows the 2D-configuration of the problem geometry. Due to the airtightness of the nacelle, the physical problem splits into two independent parts: internal and external sub-problems. In the internal sub-problem, heat transfer occurs by confined natural convection and by radiation within the nacelle. Whereas in the external sub-problem, heat exchange of the nacelle with the surroundings occurs by radiation and by forced convection of the axial air flowing over the nacelle.

To solve the internal sub-problem, the CFD (Computational Fluid Dynamics) method is used. On the other hand, a suitable correlation taken from the literature is used to approach the external sub-problem. The following practical considerations and simplifying assumptions are adopted:

- Both 2D and 3D-cases are tackled in the present work;
- Non-stationary turbulent regime is considered;
- Heat transfer by radiation is considered inside and outside the nacelle;
- The effect of gravity (buoyancy force) is considered. Therefore, heat transfer by confined natural convection occurs within the nacelle;
- Heat generation (released mainly by the electrical generator) is idealized as an isothermal condition, represented by a hot plate at temperature T_H;
- The cooling system is idealized as an isothermal condition, represented by a cold plate (i.e. the nacelle cover) at the cooling temperature T_C;
- The external air flow is assumed to be horizontal with a constant free stream temperature T_{ext} and a constant horizontal velocity U_∞, where the blades and

tower effect on the air flow is neglected.

2.2. Governing equations

The complete set of fluid equations, expressed in the Cartesian coordinate system, consists of the unsteady Reynolds-averaged Navier-Stokes and energy equations, where Boussinesq approximation is considered for the temperature-density dependence.

$$\frac{\partial u_i}{\partial x_i} = 0, \tag{1}$$

$$\frac{\partial u_i}{\partial t} + u_j \frac{\partial u_i}{\partial x_j} = -\frac{1}{\rho}\frac{\partial p}{\partial x_i} + \frac{\partial}{\partial x_j}\left[\nu\left(\frac{\partial u_i}{\partial x_j} + \frac{\partial u_j}{\partial x_i}\right) - \overline{u_i' u_j'}\right] - g\beta\delta_{i2}(T - T_0), \tag{2}$$

$$\frac{\partial T}{\partial t} + u_j \frac{\partial T}{\partial x_j} = \frac{\partial}{\partial x_j}\left(\alpha \frac{\partial T}{\partial x_j} - \overline{u_i' T'}\right), \tag{3}$$

where, u_i is the mean velocity component in the x_i direction, and u_i' is the corresponding fluctuating velocity component. p is the pressure, T is the air mean temperature and T' is the corresponding fluctuating temperature. t denotes the time variable. ρ, ν, α and β denote respectively density, kinematic viscosity, thermal diffusivity and thermal expansion coefficient of the air. g is the acceleration due to gravity and T_0 is a reference temperature given by $T_0 = (T_H + T_C)/2$. δ_{ij} is the Kronecker delta symbol.

For turbulence modeling, the Reynolds stresses $\overline{u_i' u_j'}$ and the turbulence heat fluxes $\overline{u_i' T'}$ are modeled through the Boussinesq approximation as follows.

$$\overline{u_i' u_j'} = -\frac{\mu_t}{\rho}\left(\frac{\partial u_i}{\partial x_j} + \frac{\partial u_j}{\partial x_i}\right) + \frac{2}{3}k\delta_{ij}, \tag{4}$$

$$\overline{u_i' T'} = -\frac{\mu_t}{\rho\sigma_T}\frac{\partial T}{\partial x_i}, \tag{5}$$

where μ_t denotes the turbulent eddy viscosity, k is the turbulent kinetic energy and σ_T is the turbulent Prandtl number. The shear-stress transport (SST) $k-\omega$ model with four additional transport equations has been considered for turbulence modeling. As it has been shown by Wu & Lei (2015), this model has the best performance in terms of predicting turbulence quantities in confined natural convection. Further details of this model can be found in Wilcox (1994).

2.3. Radiation modeling

Air within the nacelle is transparent and assumed to be non-absorbing and non-emitting, therefore it is considered as non-participating medium. The nacelle cover and the generator wall are assumed to be gray, opaque and diffuse emitters and reflectors of radiation with an emissivity of $\epsilon = 0.9$. For such conditions, the surface-to-surface radiation model (S2S) is selected to account for the heat transfer by radiation within the nacelle, where the view factor related to the elementary surfaces i and j, of the

respective areas dA_i and dA_j, separated by a distance r is calculated as

$$F_{ij} = \frac{1}{A_i} \int_{A_i} \int_{A_j} \frac{\cos\theta_i \cos\theta_j}{\pi r^2} \chi_{ij} \mathrm{d}A_i \mathrm{d}A_j, \tag{6}$$

where θ_i and θ_j are the angles between the normals of the elementary surfaces and the ray separating them. The factor χ_{ij} is equal to 1 if $\mathrm{d}A_j$ is visible to $\mathrm{d}A_i$, and 0 otherwise.

3. Numerical method

3.1. Computational domain and boundary conditions

As it will be explained in the next sections, heat exchange with the surroundings is modeled through a suitable correlation. Therefore, only the nacelle inner part constitutes the computational domain. Figure 2 shows the associated boundary conditions. For the temperature field, the isothermal conditions are prescribed on the internal wall of the nacelle cover (i.e. cold plate at T_C) and on the electrical generator wall (i.e. hot plate at T_H). The non-slip conditions are prescribed for the velocity field.

For a detailed investigation of temperature and air flow fields in the 2D-case, two longitudinal lines, A and B, and two transversal lines, C and D, have been considered. Also, a vertical upward-oriented path $\mathcal{E}$, of a center $\mathcal{Q}$, lying on the left-mid-plane between hot and cold plates is considered (cf. Fig. 2). Furthermore, to investigate the 3D-case, it is instructive to consider two vertical YZ-plane sections (I) and (II) passing respectively through the transversal lines C and D.

3.2. Numerical formulation

To solve the resulting governing equations along with the specified boundary conditions, ANSYS FLUENT code based on the finite-volume method has been used where PISO algorithm is employed for the pressure-velocity coupling. All the equations have been discretized using the second-order upwind differencing scheme. The discretized equations have been iterated with a relaxation factors of 0.9 for the energy equation and 1 for all the other equations. As an exception, for the 3D-case, it has been noticed that convergence requires a relaxation factor of 0.7 for the pressure equation. On the other hand, it is known that numerical resolution of transient confined natural convection problems require high CPU time simulations. This issue has been pointed by many authors dealing with the problem of time-dependent natural convection within enclosures, e.g. Ben Cheikh et al. (2007).

3.3. Grid topology

Structured rectangular meshes have been used to carry out simulations. Fine grid is considered close to the isothermal walls where high temperature and velocity gradients take place. Figure 3 shows the topology of the 2D-grid. Results of mesh and time-step dependency study are presented in the next section.

4. Results and discussions

4.1. Problem statement

To investigate the thermal behavior of the wind turbine nacelle, a typical $850kW$ commercial wind turbine has been considered. The geometry of the nacelle has been simplified into a horizontal circular cylinder of $13m \times 3m$, inside of which lies a coaxial cylindrical generator of $3.22m \times 1.4m$ placed at a distance of $0.48m$ from the back side of the nacelle (cf. Fig. 1). Hot plate temperature T_H is maintained constant at a safety limit of $100°C$ in all this study. Therefore, the temperature span $\Delta T = T_H - T_C$ is controlled only by varying the cooling temperature T_C. It is of interest to notice that for such dimensions of the nacelle and for temperature span ΔT varying in the range of $120°C \rightarrow 70°C$, Rayleigh number based on the longest distance between hot and cold plates, that is length of Line A, is $Ra_A \sim 10^{12}$ which would keep the air flow inside the nacelle within highly turbulent regime level. In such conditions, a time-dependent approach is required.

For the external sub-problem, typical values of $55°C$ and $5m/s$ are considered for the temperature and the velocity of the free stream air, respectively.

4.2. Mesh and time-step dependency study

To determine the optimal grid and time-step size that would produce accurate results with efficient CPU-time simulations, computations have been performed for typical boundary conditions. The resulting total heat rate exchanged within the nacelle, q_{int}, given by Eq. (7), has been calculated near hot and cold plates, by considering different grid dimensions and time-step sizes.

$$q_{int}^{H/C} = \int_{\mathcal{H}/\mathcal{C}} k \left.\frac{\partial T}{\partial n}\right|_{\mathcal{H}/\mathcal{C}} ds, \tag{7}$$

where $\mathcal{H}$ and $\mathcal{C}$ denote the curvilinear paths describing hot and cold plates, respectively. n and s are the local coordinate normal to the wall and the curvilinear coordinate, respectively. k is the air thermal conductivity assumed to be constant and calculated at the reference temperature T_0.

Several grids with different number of nodes have been employed to discretize the computational domain. Figure 4 shows a flowchart diagram summarizing the steps sequence and logic of the mesh and time-step dependency study. As it can be seen, the flowchart logic is structured in two main parts where two simulation parameters are to be determined; the grid nodes optimal number, N^*, and the optimal time-step size, τ^*.

After initialization of the grid nodes number, N, and the time-step size, τ, simulation is run and the transient evolution of the total heat rates, q_{int}^H and q_{int}^C, is tracked. If a smooth and not-wiggling transient evolution is noticed, then equations are iterated until reaching the steady-state regime, characterized by an almost energy-balanced state, i.e. $q_{int}^H \approx q_{int}^C$. In all simulations, for each grid and each time-step size, the steady-state regime criterion is set to be based on the relative difference between q_{int}^H and q_{int}^C (i.e., $(q_{int}^H - |q_{int}^C|)/q_{int}^H < \varepsilon_1$, with $\varepsilon_1 = 1.2\%$). Then, the total heat rate, q_{int}, is recorded and the mesh is refined repeatedly until reaching a convergence ratio of $\varepsilon_2 = 1.0\%$. The same strategy is applied for the time-step dependency over a decreasing range of time-step sizes, where a tinier value of 0.1% is considered for the convergence

ratio, ε_3. Figure 5 shows in the same plot the results of both mesh and time-step size dependency study. As it can be seen, for a number of nodes greater than 6×10^4, the resulting values of the total heat rate seem to be almostly independent to the grid size. On the other hand, the obtained optimal value of the time-step size is $10^{-3}s$.

The same study has been conducted for the 3D model. The optimal number of grid nodes has been found to be equal to 5×10^5, whereas a nearly unchanged value of $10^{-3}s$ is obtained for the optimal time-step size.

The computer system used to run the calculations has 32GB of RAM and an i7-4790 processor with a total of 8 core Intel processors, each running 3.60GHz. Computations have been conducted over an average of about 5.5×10^5 time-steps, corresponding to a physical time of 4 days for each simulation.

4.3. Temperature field and streamline contours

Figure 6 shows the resulting temperature distribution and streamline contours in the 2D-case obtained for cold and hot plate temperature values of $T_C = 0°C$ and $T_H = 100°C$. As it can be seen, the behavior of these results seems to be quite reasonable, thus confirming, qualitatively, the validity of the proposed numerical method. In particular, the thermal stratification phenomenon of the air on the left side of the nacelle driven by the concentration of the hot air on the upper part of the nacelle which is due to the decrease in the density, thus confirming the suitability of the adopted Boussinesq approximation.

From Figure 6(b), it can be noticed that the air motion within the nacelle is characterized by a recirculating flow concentrated mainly in three cells adjoining the hot and cold walls. On the left-bottom side of the nacelle, thermal instability starts to occur, giving birth to secondary air circulation core.

Figure 7 shows the distribution of temperature patterns in the 3D-nacelle where the thermal stratification phenomenon of the air on the left side of the nacelle appears to be even more clear.

Figure 8 shows radial distributions of temperature and velocity fields in the YZ-plane sections (I) and (II). As it can be seen, the heated air ascends along the generator wall vicinity, then descends along the nacelle cover wall to the bottom, where the flow structure is characterized by a stagnant region.

Similar conclusions can be drawn from the results (not presented here) obtained for other temperature spans between hot and cold plates.

4.4. Temperature and velocity profiles

To visualize explicitly temperature and velocity fields within the nacelle in the 2D-case, results have been extracted along the two longitudinal lines, A and B, and the two transversal lines, C and D, previously introduced in Fig. 2. The cold plate temperature is considered to be varying from $T_C = -10°C$ to $10°C$. The obtained profiles of temperature as well as vertical and horizontal velocities are presented in Figure 9.

Figures 9(a) and (b) show profiles of temperature and vertical velocity along Line A, respectively. For different cold plate temperatures, temperature profiles behave similarly, decreasing from the common hot plate temperature T_H to the corresponding cooling temperature T_C. High air motion can be noticed, upward in the vicinity of the hot plate and downward near the cold plate. Also, it is important to notice that sharp variations occur more clearly in the vicinity of the hot plate than the opposite cold

side, because of higher temperature gradient.

Along Line B, temperature and vertical velocity profiles behave similarly to those along Line A (cf. Fig. 9(c) and (d)). However, because of the nearness of the two isothermal plates, more significant air motion can be noticed.

Figures 9(e) and (f) show profiles of temperature and horizontal velocity along Line C, respectively. As it can be seen, temperature profiles exhibit a sharp increase from the cooling temperature at the nacelle bottom to reach a maximal value in the upper part of the nacelle (92% of the nacelle height). Then, it decreases more sharply again to the cooling temperature at the top wall of the nacelle. From Figure 9(e), it is instructive to notice the linear increase of the temperature in front of the generator left wall, along the path $\mathcal{E}$, underlying again the thermal stratification phenomenon of the air in this part of the nacelle. On the other hand, as it would be expected, horizontal velocity profiles along Line C show that motion of air is definitely more significant in the vicinity of the nacelle top wall occupied by a highly heated mass of air. These behaviors confirm one more time the adopted Boussinesq approximation.

As it can be seen in Figures 9(g) and (h), along Line D, a well stratified air is noticed due to the horizontal disposition of the two isothermal plates (hot plate on the top, and cold plate on the bottom). Temperature values increase progressively from the corresponding T_C at the bottom of the nacelle to reach the common hot temperature T_H at the bottom of the generator, where high temperature and velocity gradients occur on the walls vicinity.

4.5. Analysis of the air thermal stratification phenomenon

In order to investigate quantitatively the validity of the proposed numerical method and accuracy of the 2D-case results, it is of interest to put light on the stratifying air in the widest area of the nacelle, that is the left side. For this aim, the 2D-case is considered. We focus our analysis on air flow and heat transfer in the vicinity of the generator left wall. Heated air in the vicinity of the left wall of the generator ascends upward and reaches the top cold wall of the nacelle. Further, it moves horizontally leftward, then being cooled, it moves downward and returns back to the generator hot wall. Once the steady-state regime reached, this mechanism leads to a recirculating air-flow under thermal stratification conditions (Martynenko & Khramtsov , 2011).

For different cooling temperature cases, temperature far the wall, T_∞, evaluated at the point $\mathcal{Q}$ (cf. Fig. 2), and the temperature slop along the path $\mathcal{E}$ are extracted. Next, this data is used to correlate the resulting average Nusselt number over the generator left wall, making use of Equation (8) reported by (Martynenko & Khramtsov , 2011).

$$\overline{Nu}_f = C_t Ra_f^{1/3} \frac{3}{7S_\mathcal{E}} \left[\left(\frac{2+S_\mathcal{E}}{2} \right)^{7/3} - \left(\frac{2-S_\mathcal{E}}{2} \right)^{7/3} \right]. \tag{8}$$

As recommended in (Bergman et al., 2011), the turbulence coefficient C_t is taken to be equal to 0.1. Ra_f is the Rayleigh number based on the length of the generator left wall, L_f, given by

$$Ra_f = \frac{g\beta(T_H - T_\infty)L_f^3}{\alpha\nu},$$

and $S_{\mathcal{E}}$ is the stratification parameter assessed through the path $\mathcal{E}$ and defined as

$$S_{\mathcal{E}} = \frac{L_f}{(T_H - T_\infty)} \left.\frac{\partial T}{\partial y}\right|_{\mathcal{E}}.$$

It is of interest to notice that conditions of the present problem are such that the stratification parameter lies in the interval $0 < S_{\mathcal{E}} < 2$, which is the range of validity of the correlation (8).

Table 1 shows the variation of the resulting T_∞ and the temperature slop, $\left.\frac{\partial T}{\partial y}\right|_{\mathcal{E}}$, with respect to the cooling temperatures, T_C. Also, it presents a comparison between the corresponding values of the average Nusselt number over the generator left wall obtained by the latter correlation, $\overline{Nu}_f^{\,corr.}$, and those obtained by the present numerical method, $\overline{Nu}_f^{\,pres.}$, along with the corresponding relative discrepancies.

As it can be seen, the resulting Nusselt number values averaged over the generator left wall exhibit a similar trend to those computed using Eq. (8) confirming, thus, quantitatively the validity of the numerical approach. An average under-predicting relative error of 9.6% is recorded over the whole cooling temperature range. This value is quite satisfactory, since numerical correlation errors lower than 25% may generally be considered as acceptable (Bergman et al., 2011).

4.6. Analysis of natural convection in the cylindrical annuli part of the 3D-nacelle

For further quantitative validation of the proposed method, it is of interest to put light on the accuracy of simulation results obtained in the 3D-case. For this purpose, we consider the 3D turbulent natural convection case and focus our study on the horizontal cylindrical annuli part of the nacelle. Under the present physical considerations, the Rayleigh number based on the annuli width is in the order of $Ra_D \sim 10^9$.

In order to carry out comparison with literature data, the YZ-plane section (II) has been considered. The location of this plane leads to a physical situation typically similar to the benchmark problem of turbulent natural convection in concentric horizontal annuli.

From Figure 8.II.a, temperature values are extracted along three radial directions L_i identified by the angle $\phi = \langle D, L_{i=1,2,3} \rangle = 150°, 120°$ and $90°$, respectively. Figure 10 shows the obtained results compared with the experimental data of (McLeod & Bishop, 1989) measured in the case of Rayleigh number equal to 1.9×10^9. Temperature and radial coordinate are non-dimensionalized such that $\overline{T} = (T - T_C)/(T_H - T_C)$ and $\overline{r} = (r - r_i)/(r_o - r_i)$, where r_i and r_o are, respectively, the inner and the outer cylinders radii.

As it can be seen, the numerical method adopted in the present study predicts, in general, an acceptable radial distributions of the temperature in the midplane of the annuli part of the 3D-nacelle. However, a conspicuous overestimation can be noticed particularly near the hot plate wall. This discrepancy is expected and might be explained by the slight difference between the respective Rayleigh numbers.

4.7. Nacelle thermal behavior analysis

To investigate properly the nacelle thermal behavior, two key parameters are assessed: the resulting average temperature of the air within the nacelle, T_{av} , calculated as

$$T_{av} = \frac{1}{\Omega} \int_{\Omega} T d\Omega, \tag{9}$$

where Ω denotes the inner volume of the nacelle, and the cooling capacity required for the cooling process, q_C, that is to be determined through the energy balance equation

$$q_C = q_{int} + q_{ext}, \tag{10}$$

where, q_{int} is the heat rate released by the electrical generator calculated numerically using Eq. (7). q_{ext} is the heat rate exchanged with the surroundings by radiation and by forced convection, such that

$$q_{ext} = \sigma \mathcal{A} \left(T_{sky}^4 - T_C^4 \right) + h \mathcal{A} \left(T_{ext} - T_C \right), \tag{11}$$

with σ being the Stefan-Boltzmann constant and $\mathcal{A}$ the area of the nacelle cover. Under typical Saharan weather conditions (cloudless sky, low humidity), the sky temperature T_{sky} can be taken to be equal to $-50°C$.

In order to determine the convection heat transfer coefficient h, heat exchange with the surroundings is modeled using the following correlation

$$Nu = 0.155\,\mathrm{Re}^{0.674}, \tag{12}$$

where Nu is the Nusselt number averaged over the cylinder surface, defined by $Nu = hD/k$, and Re is the Reynolds number based on the cylinder diameter given by $\mathrm{Re} = U_\infty D/\nu$. This correlation is proposed by (Wiberg & Lior, 2005) to correlate the case of a horizontal circular cylinder placed in an upstream axial flow affected by a turbulence-generating grid. For the purpose of the present study, this correlation is suitable since the nacelle is long enough to make the reattachment length of the turbulent flow lower than the nacelle length.

Figures 11 and 12 show, respectively, the evolution of the resulting exchanged external and internal heat rates both in 2D and 3D-configurations, where the different modes of heat transfer occurring outside and inside the nacelle are discerned (forced convection and radiation outside the nacelle, natural convection and radiation inside the nacelle). We notice that the external heat exchange contribution constitutes the main part (about 80%) of the total resulting thermal loads to be balanced by the cooling system. This result confirms the drastic impact of the Saharan weather conditions on the thermal behavior of the nacelle.

However, it is of interest to notice that the convective activity of the air within the nacelle affects the nacelle thermal behavior more intensively as the cooling temperature decreases. Therefore, the contribution of the internal heat exchange by radiation and by natural convection constitutes an important factor not to be neglected during the thermal design of the nacelle cooling system.

As it can be seen, all the resulting heat rates exhibit linear regression with respect to the cooling temperature. Moreover, within the nacelle, heat exchange by radiation seems to be more significant than by convection. In fact, it has been found that it

constitutes more than 73% of the internal thermal loads both in 2D and 3D cases. This result agrees well with the conclusion previosely drawn by the authors who investigated conjugate heat transfer by natural convection and radiation in cavities, e.g. (Liu & Phan-Thien, 1999), (Baïri et al., 2014). Whereas, for the outer side of the nacelle, it is the heat rate by convection that presents the main part of the resulting external thermal loads.

Figure 13 shows the evolution of the average temperature within the nacelle, where effects of heat transfer by convection alone and by conjugate convection and radiation are compared. As it can be seen, the resulting average temperature in the 3D case is slightly lower, which might be explained by the relatively more considerable thermal mass of air within the nacelle in this case.

Figure 14 shows the evolution of the required cooling capacity with respect to the cooling temperature. As it can be seen, the lower is the cooling temperature, the more energy-requiring is the cooling process. This is again a qualitative validation of the numerical method.

From the previous data, in order to assess properly the thermal behavior of the nacelle, the resulting heat rates inside and outside the nacelle as well as the required cooling capacity can be correlated linearly to the resulting average temperature within the nacelle. Table 2 displays the coefficients of the corresponding linear correlations, where the case of conjugate heat transfer by convection and radiation is considered both in 2D and 3D-cases .

5. Conclusion

This paper presents a numerical method to investigate the thermal behavior of a HAWT nacelle under the effect of conjugate heat transfer by convection and radiation. For this purpose, an air-tight nacelle has been considered. The heat generation and the cooling system idealized as isothermal conditions have been represented respectively by hot and cold plates in the computational domain. The problem has been split into inner sub-problem investigated numerically and outer sub-problem approached using a suitable correlation.

Simulations have been carried out both in 2D and 3D-cases for different cooling temperatures. The resulting profiles of temperature and velocity have been visualized along different directions within the nacelle, and shown good agreement with the results found in the literature.

To investigate the validity of the 2D-results, an analysis of the thermal stratification phenomenon of the air within the nacelle has been carried out: For different cooling temperatures, the resulting average Nusselt number over the generator left wall has been compared with the correlation results provided by the literature, where a satisfying agreement has been noticed.

The 3D-case results have been validated by putting light on the heat transfer by turbulent natural convection in the cylindrical annuli part of the nacelle. Temperature profiles have been extracted over different radial directions, where the comparison with experimental data found in the literature has shown an acceptable concordance.

The thermal behavior of the nacelle has been assessed both in 2D and 3D-cases by considering two parameters: the required cooling capacity and the resulting average temperature within the nacelle. It has been noticed that these two parameters exhibit a linear evolution with respect to the cooling temperature. Analysis of the obtained data has confirmed that appropriate values of the required cooling loads are definitely

dependent on the accurate predictions of the internal heat exchange by radiation and by natural convection within the nacelle. However, it has been found that the external heat exchange of the nacelle with the surroundings constitutes the main part of the thermal loads to be balanced by the cooling system (about 80%), which confirms the drastic impact of the Saharan climate on the thermal behavior of the nacelle.

Future works will be mainly focused on the consideration of more practical aspects for the thermal design of the nacelle; namely the unsteady thermal loads due to generator, gearbox and electronic components. Numerical computations of the external heat exchange of the nacelle with the surroundings and the flow fields around the nacelle will be carried out using the CFD method, where the aerodynamic shape of the nacelle may constitute an important parameter.

Acknowledgments

Computer Science and Engineering Department of University of Minnesota and the Algerian Government are gratefully acknowledged for their sponsorship and resources. The work of Yousef Saad was supported by NSF under grant 1521573.

Disclosure statement

We confirm that there are no known conflicts of interest associated with this publication.

References

C. Arzbaecher, K. Parmenter, E. Fouche, Industrial waste-heat recovery: Benefits and recent advancements in technology and applications, 2007 ACEEE Summer Study on Energy Efficiency in Industry, European Council for an Energy Efficient Economy, Stockholm, Sweden.

A. Baïri, E. Zarco-Pernia, J.-M. García de María, A review on natural convection in enclosures for engineering applications. The particular case of the parallelogrammic diode cavity, App. Th. Eng. 63 (2014) 304-322.

N. Ben Cheikh, B. Ben Beya, T. Lili, Benchmark solution for time-dependent natural convection flows with an accelerated full-multigrid method, Num. Heat transfer, Part B 52 (2007) 131-151.

C.C. Chen, R. Eichhorn, Natural convection from a vertical surface to a thermally stratified fluid, Journal of Heat Transfer (1976) 446-451.

C.P. Chiu, W.R. Chen, Transient natural convection heat transfer between concentric and vertically eccentric spheres, Int. J. Heat Mass Transfer 39 (7) (1996) 1439-1452.

D.C. Wilcox, Turbulence Modeling for CFD, DCW Industries, California, USA (1994).

B. Farouk, S.I. Güçeri, Laminar and turbulent natural convection in the annulus between horizontal concentric cylinders, Jour of Heat Transfer 104 (1982) 631-636.

T.L. Bergman, A.S. Lavine, F.P. Incropera, D.P. Dewitt, Fundamentals of heat and mass transfer, Seventh edition, John Wiley & Sons (2011).

P. Łapka, M. Bakker, P. Furmański, H. van Tongeren, Comparison of 1D and 3D thermal models of the nacelle ventilation system in a small airplane, Aircraft Engineering and Aerospace Technology, 90 (1) (2018) 114–125.

C.-C. Liao, C.-A. Lin, Transitions of natural convection flows in a square enclosure with a heated circular cylinder, App. Th. Eng. 72 (1) (2014) 41-47.

Y. Liu, N. Phan-Thien, A complete conjugate conduction convection and radiation problem for a heated block in a vertical differentially heated square enclosure, Comput. Mech. 24 (1999) 175-186.
J. Ma, F. Xu, Unsteady natural convection and heat transfer in a differentially heated cavity with a fin for high Rayleigh numbers, App. Th. Eng. 99 (2016) 625-634.
M. A. Mahdi, A. Smaili, Numerical investigations of laminar buoyant heat transfer in a 2D-enclosure — Application to wind turbine nacelle operating in hot climate, Mechanika 23 (5) (2017) 667-672.
M. A. Mahdi, A. Smaili, Numerical investigations of the thermal behavior of a HAWT nacelle using ANSYS FLUENT, Energy Procedia 141 (2017) 394-398.
A.E. McLeod, E.H. Bishop, Turbulent natural convection of gases in horizontal cylindrical annuli at cryogenic temperatures, Int. Jour. of Heat and Mass Transfer 32 (1989) 1967-1978.
A. Mezrhab, H. Bouali, H. Amaoui, M. Bouzidi, Computation of combined natural-convection and radiation heat-transfer in a cavity having a square body at its center, App. Energy 83 (2006) 1004-1023.
Y. Miki, K. Fukuda, N. Taniguchi, Large eddy simulation of turbulent natural convection in concentric horizontal annuli, Int. Jour. of Heat and Fluid Flow 14 (3) (1993) 210-216.
M. Montiel-Gonzáleza, J.F. Hinojosab, H.I. Villafán-Vidalesc, A. Bautista-Orozcoc, C.A. Estradac, Theoretical and experimental study of natural convection with surface thermal radiation in a side open cavity, App. Th. Eng. 75 (2015) 1176-1186.
G. Pechlivanoglou, S. Fuehr, C.N. Nayeri, C.O. Paschereit, The effect of distributed roughness on the power performance of wind turbines, In Proceedings of the ASME Turbo Expo., Glasgow, UK, 14-18, June 2010, 845-855.
S. Saravanan, C. Sivaraj, Coupled thermal radiation and natural convection heat transfer in a cavity with a heated plate inside, Int. Jour. Heat Fluid Flow 40 (2013) 54-64.
A. Sergent, S. Xin, P. Joubert, P. Le Quéré, J. Salat, F. Penot, Resolving the stratification discrepancy of turbulent natural convection in differentially heated air-filled cavities —Part I: Reference solutions using Chebyshev spectral methods, Int. J. Heat Fluid Flow 39 (2013) 1–14.
A. Sergent, P. Joubert, S. Xin, P. Le Quéré, Resolving the stratification discrepancy of turbulent natural convection in differentially heated air-filled cavities Part II: End walls effects using large eddy simulation, Int. J. Heat Fluid Flow 39 (2013) 15–27.
A. Smaili, C. Masson, S.R. Taleb, L. Lamarche, Numerical study of thermal behavior of a wind turbine nacelle operating in a Nordic climate, Num. Heat Trans, Part B: Fundamentals 50 (2) (2006) 121-141.
A. Smaili, A. Tahi, C. Masson, Thermal analysis of wind turbine nacelle operating in Algerian Saharan climate, En. Procedia 18 (2012) 187-196.
O.G. Martynenko, P.P. Khramtsov, Free-convective heat transfer: With many photographs of flows and heat exchanger, Springer Berlin Heidelberg (2005).
H. Sun, F. Chénier, G. Lauriat, Effect of surface radiation on the breakdown of steady natural convection flows in a square, air-filled cavity containing a centered inner body, App. Th. Eng. 31 (2011) 1252-1262.
B. Tammelin, M. Cavaliere, H. Holttinen, C. Morgan, H. Seifert, K. Säntti, Wind Energy Production in Cold Climate, Meteorological Publications, Finnish Meteorological Institute 41 (2000) Helsinki, Finland.
R. Wiberg, N. Lior, Heat transfer from a cylinder in axial turbulent flows, Int. Jour. of Heat and Mass Transfer 48 (2005) 1505-1517.
T. Wu, C. Lei, On numerical modelling of conjugate turbulent natural convection and radiation in a differentially heated cavity, Int. Jour. of Heat and Mass Transfer 91 (2015) 454-466.
S. Xin, J. Salat, P. Joubert, A. Sergent, P. Joubert, F. Penot, P. Le Quéré, Resolving the stratification discrepancy of turbulent natural convection in differentially heated air-filled cavities. Part III: A full convection-conduction-surface radiation coupling, Int. J. Heat Fluid Flow 42 (2013) 33–48.

G. Xydis, G. Pechlivanoglou, N.C. Nayeri, Wind turbine waste heat recovery — A short-term heat loss forecasting approach, Challenges 6 (2015) 188-201.

List of Figures

1 2D-configuration of the physical problem. 17
2 Computational domain and boundary conditions. 18
3 Grid topology. 19
4 Flowchart diagram for mesh and time-step dependency study. 20
5 Mesh and time-step dependency study. 21
6 (a) Temperature ($°C$) distribution, and (b) Streamline contours ($\times 10^{-3} kg/s$) within the 2D-nacelle. 22
7 Temperature distribution within the 3D-nacelle ($°C$). 23
8 Radial distributions of (a) temperature in ($°C$) and (b) velocity in (m/s) over the YZ-plan sections (I) and (II). 24
9 Distributions of (a,c,e,g) temperature, (b,d) vertical and (f,h) horizontal velocity along Lines A, B, C and D, respectively, for different cooling temperatures. 25
10 Radial distribution of the non-dimensionalized temperature in the mid-plane of the 3D-nacelle annuli part (i.e., plane section II) compared with the experimental data of McLeod & Bishop (1989). 26
11 Evolution of the exchanged heat rates by forced convection and by radiation with the surroundings as functions of the cooling temperature in 2D and 3D configurations. 27
12 Evolution of the exchanged heat rates by natural convection and by radiation within the nacelle as functions of the cooling temperature in 2D and 3D configurations. 28
13 Evolution of the averge temperature within the 2D/3D nacelle configurations as functions of the cooling temperature: comparison between convecion alone, and conjugate convection and radiation cases. 29
14 Evolution of the required cooling capacity as function of the cooling temperature both in 2D and 3D-cases. 30

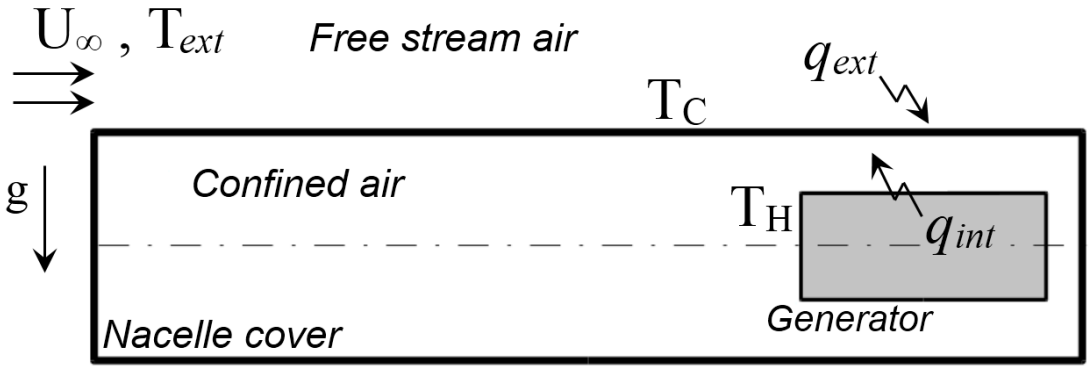

Figure 1. 2D-configuration of the physical problem.

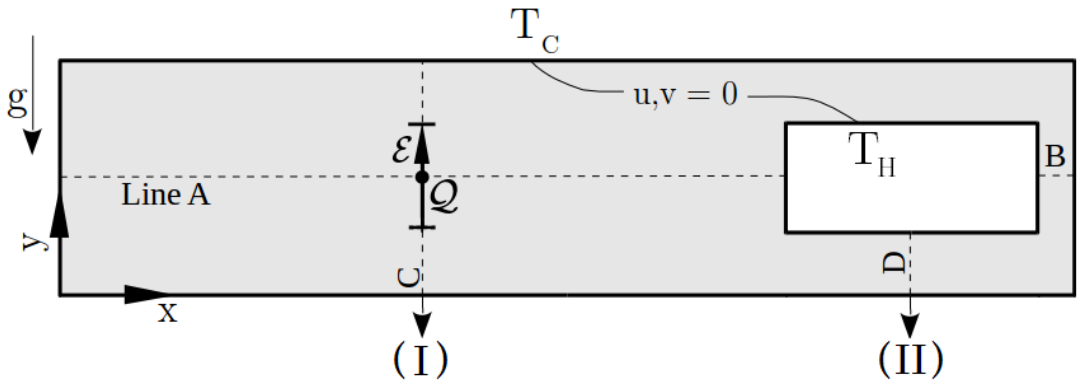

Figure 2. Computational domain and boundary conditions.

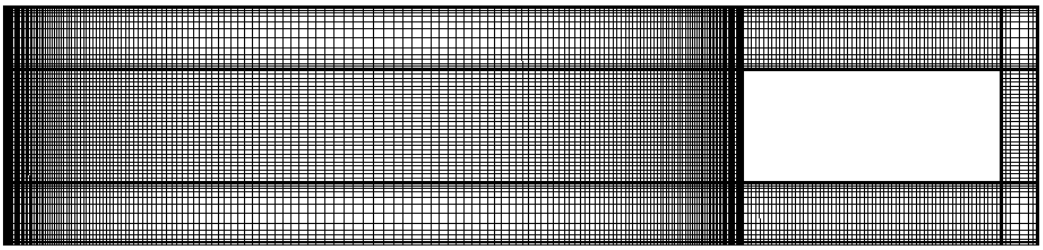

Figure 3. Grid topology.

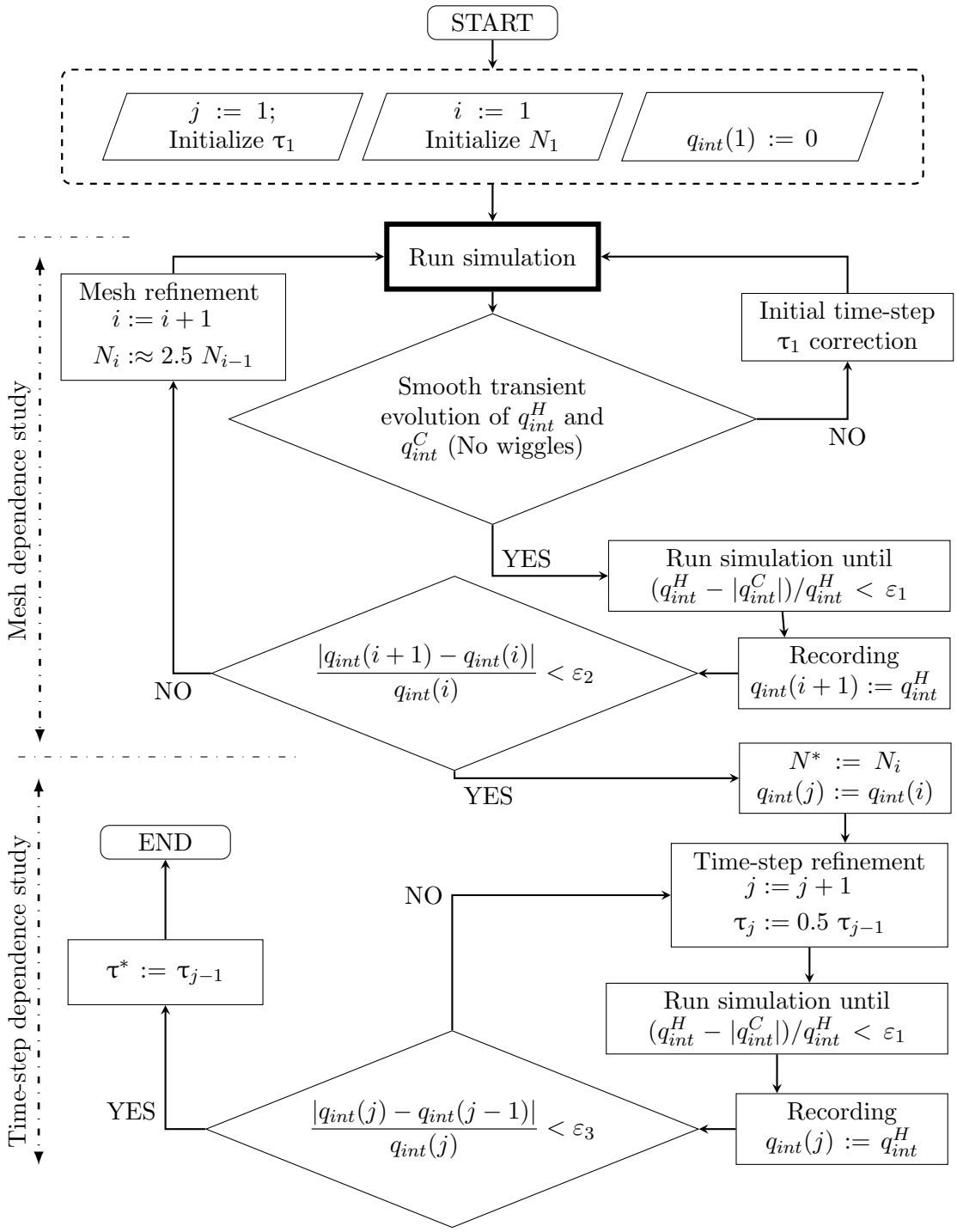

Figure 4. Flowchart diagram for mesh and time-step dependency study.

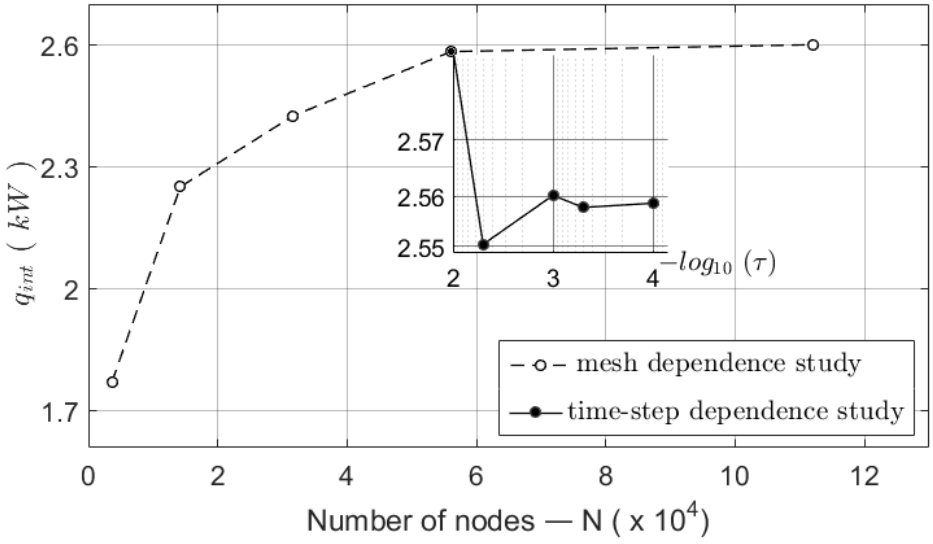

Figure 5. Mesh and time-step dependency study.

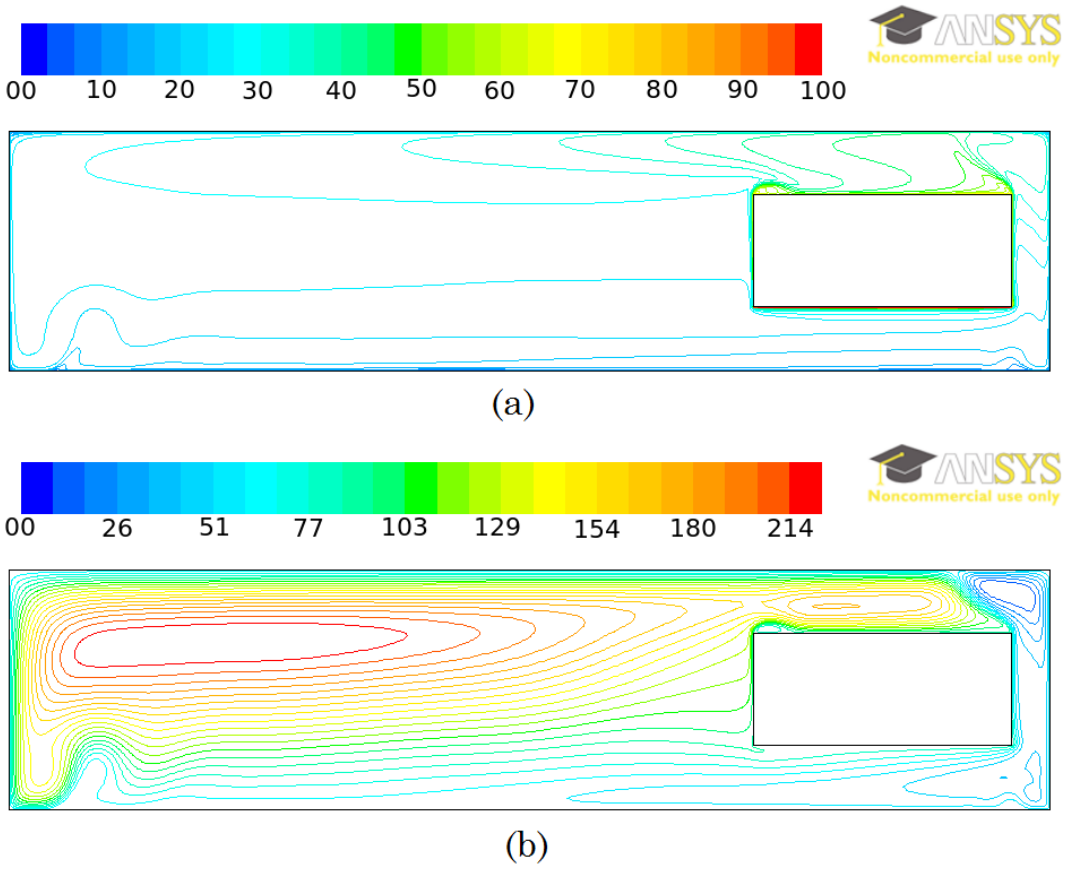

Figure 6. (a) Temperature ($^{\circ}C$) distribution, and (b) Streamline contours ($\times 10^{-3} kg/s$) within the 2D-nacelle.

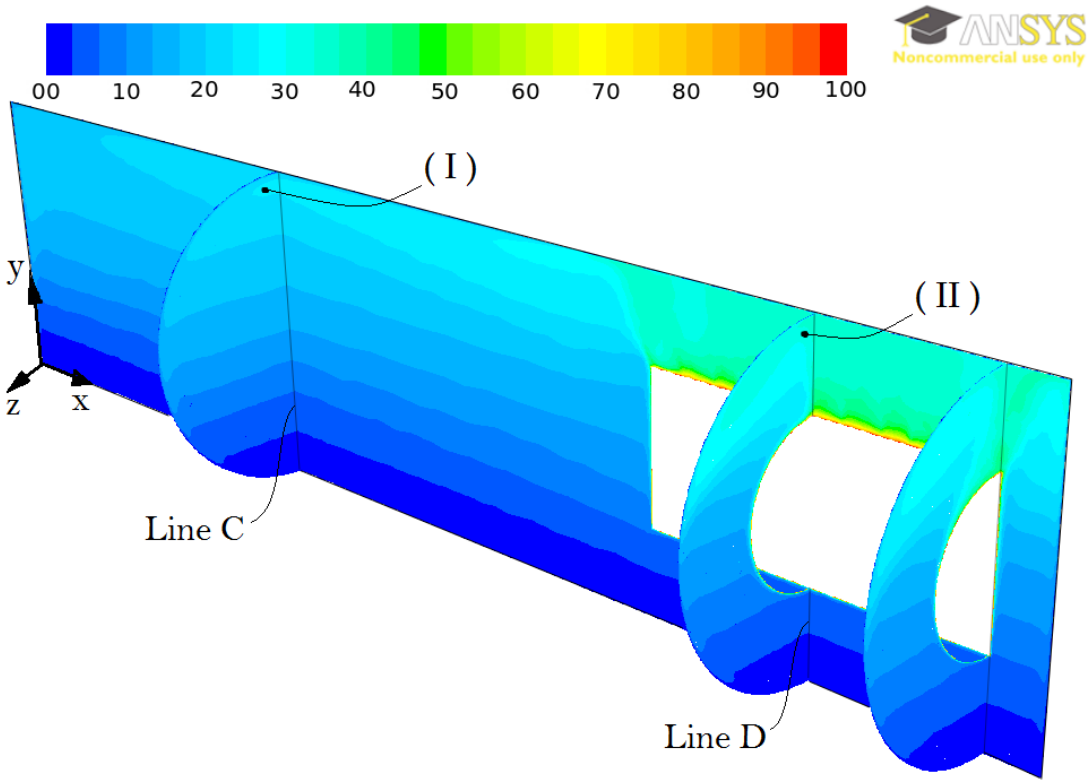

Figure 7. Temperature distribution within the 3D-nacelle ($°C$).

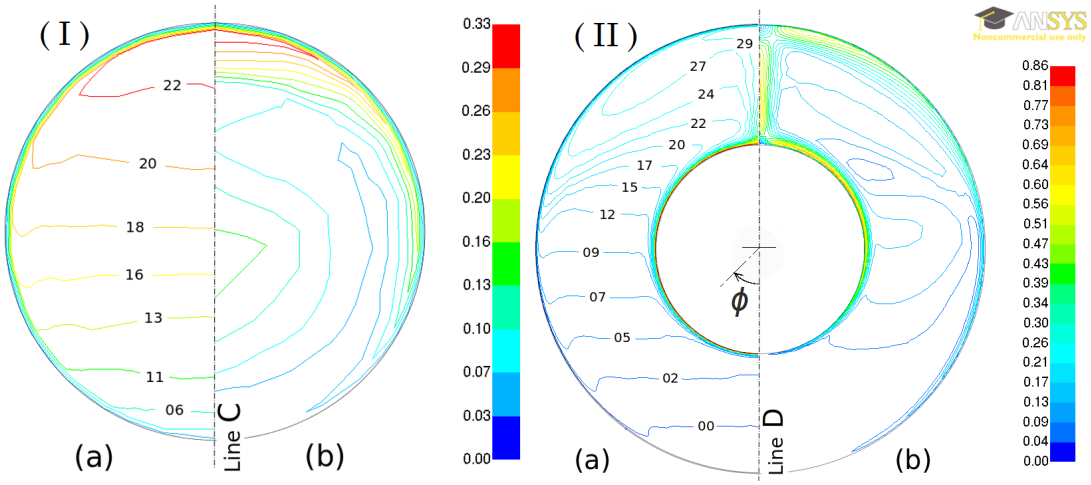

Figure 8. Radial distributions of (a) temperature in ($^{\circ}C$) and (b) velocity in (m/s) over the YZ-plan sections (I) and (II).

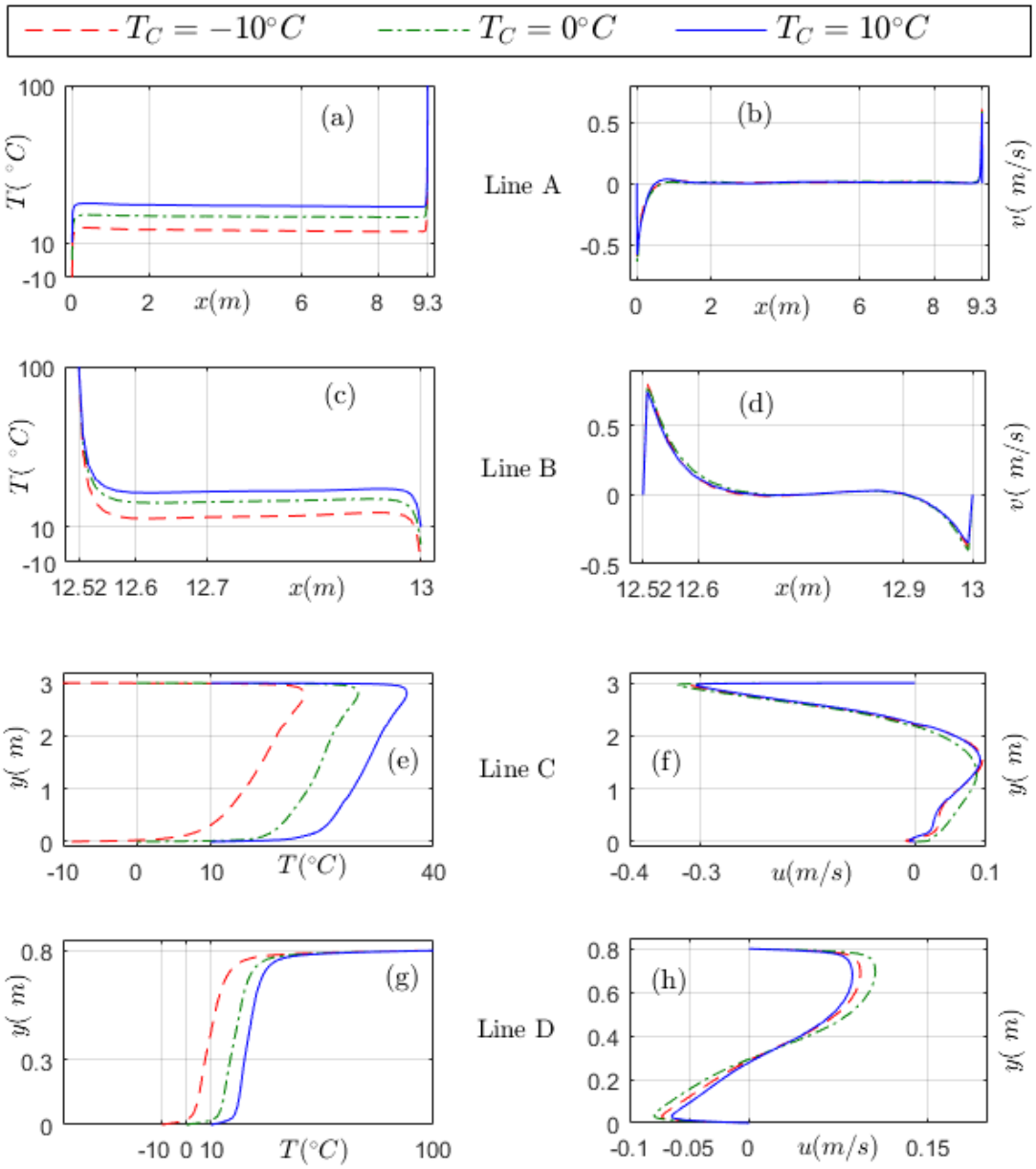

Figure 9. Distributions of (a,c,e,g) temperature, (b,d) vertical and (f,h) horizontal velocity along Lines A, B, C and D, respectively, for different cooling temperatures.

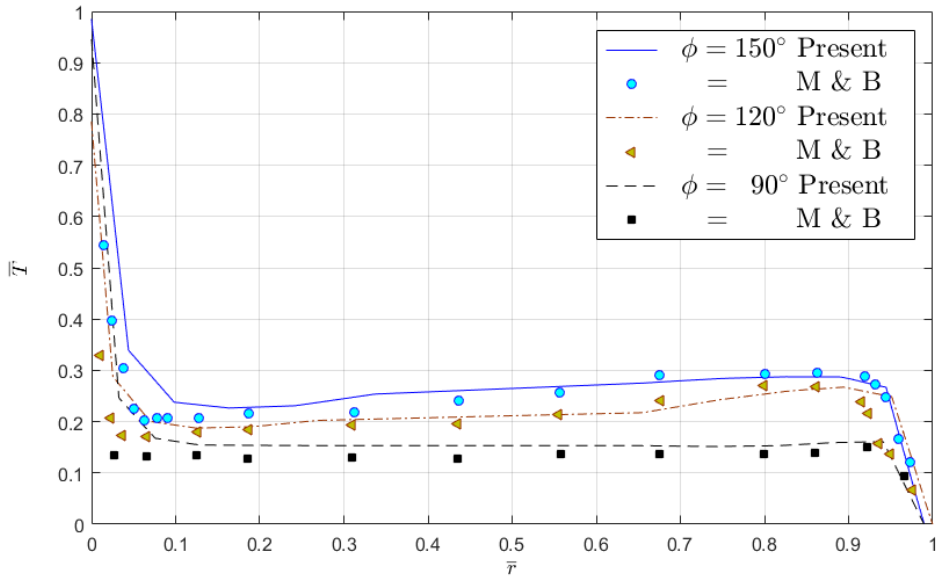

Figure 10. Radial distribution of the non-dimensionalized temperature in the midplane of the 3D-nacelle annuli part (i.e., plane section II) compared with the experimental data of McLeod & Bishop (1989).

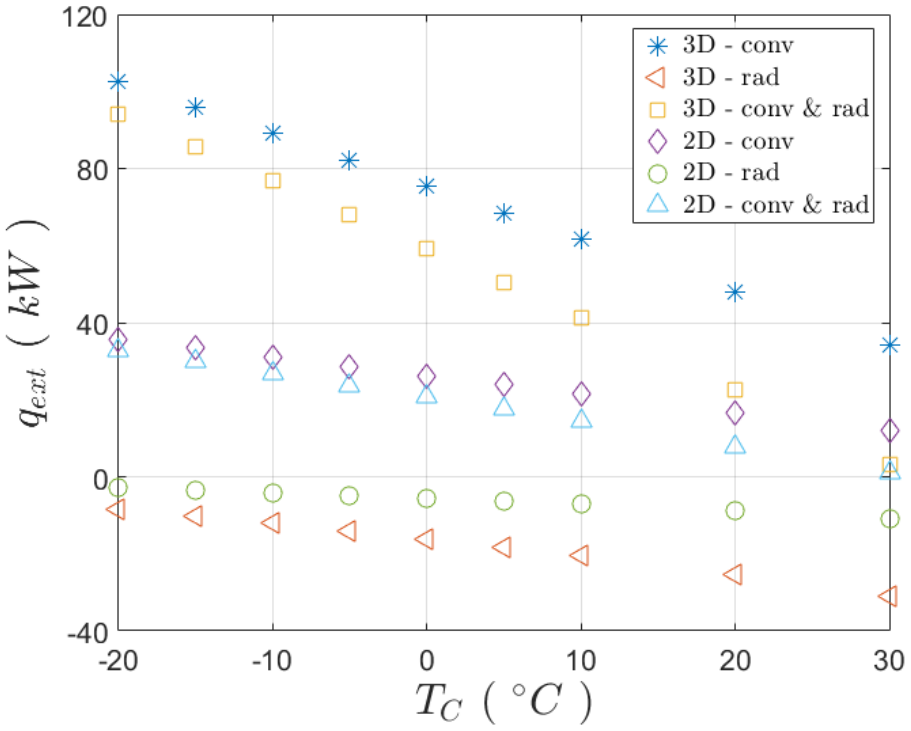

Figure 11. Evolution of the exchanged heat rates by forced convection and by radiation with the surroundings as functions of the cooling temperature in 2D and 3D configurations.

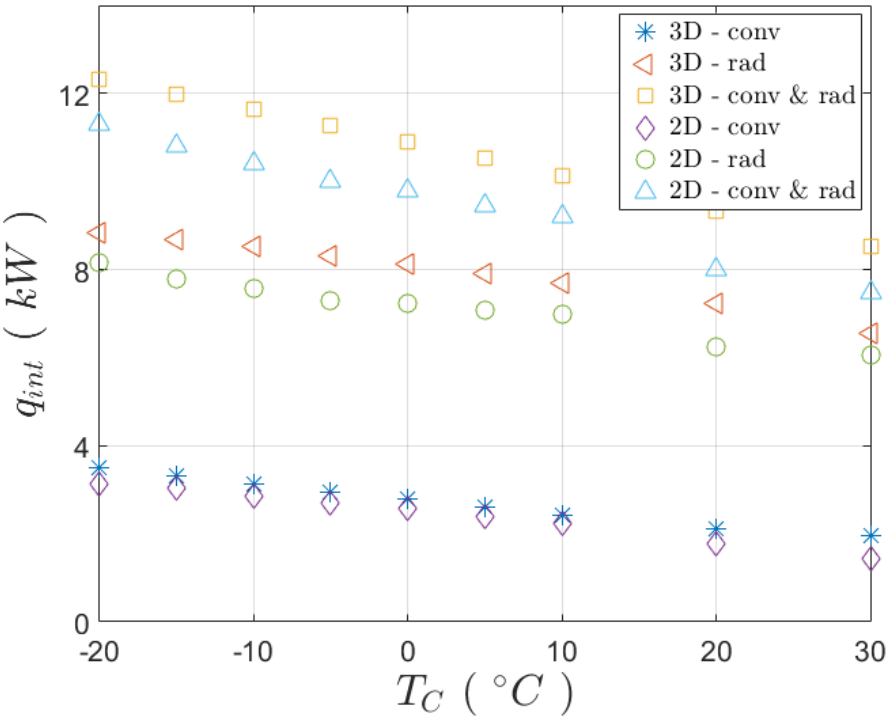

Figure 12. Evolution of the exchanged heat rates by natural convection and by radiation within the nacelle as functions of the cooling temperature in 2D and 3D configurations.

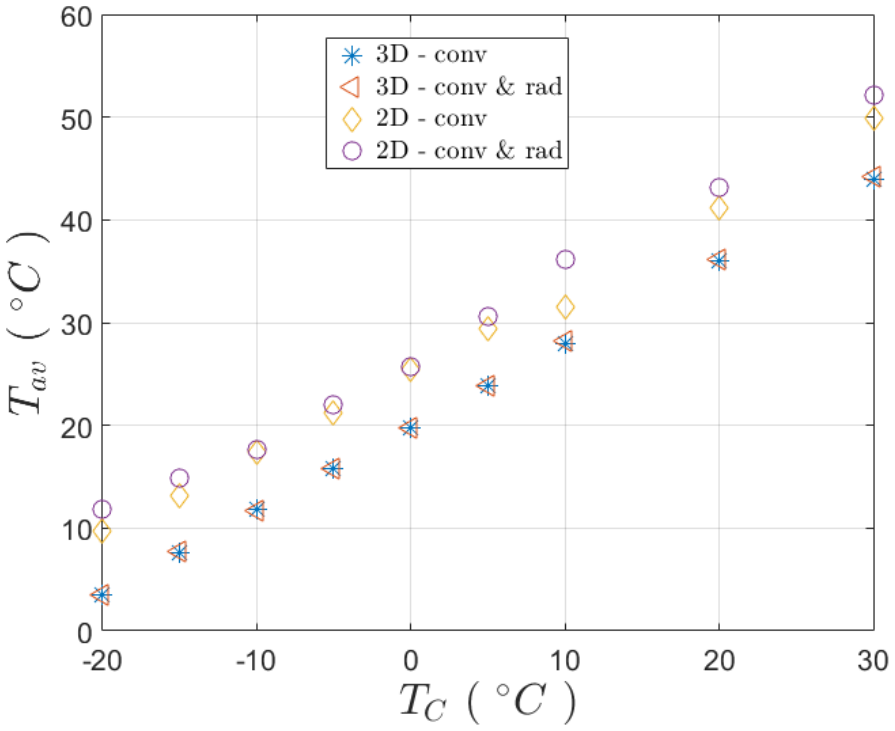

Figure 13. Evolution of the averge temperature within the 2D/3D nacelle configurations as functions of the cooling temperature: comparison between convecion alone, and conjugate convection and radiation cases.

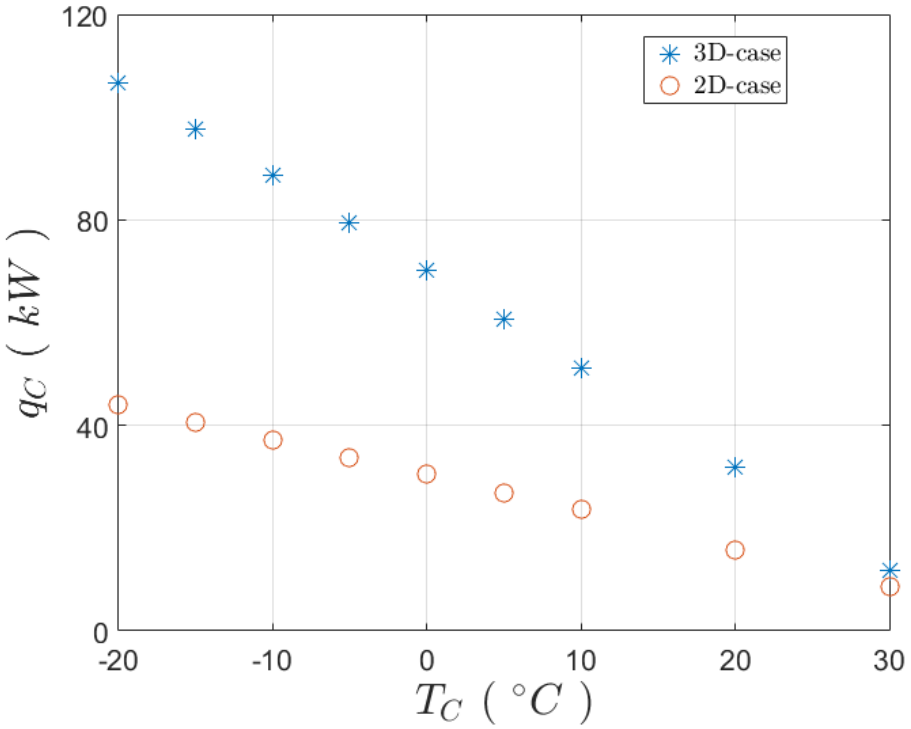

Figure 14. Evolution of the required cooling capacity as function of the cooling temperature both in 2D and 3D-cases.

List of Tables

1 Variation of Nusselt number averaged over the generator left wall . . . 32
2 Correlation coefficients of the resulting internal and external heat rates and the required cooling capacity (kW) as functions of the average temperature ($^{\circ}C$) within the nacelle : $q = \alpha\ T_{av} + \beta$ 33

Table 1. Variation of Nusselt number averaged over the generator left wall

$T_C(^\circ C)$	$T_\infty(^\circ C)$	$\frac{\partial T}{\partial y}\Big\vert_{\mathcal{E}}\left(\frac{K}{m}\right)$	$\overline{Nu}_f^{corr.}$	$\overline{Nu}_f^{pres.}$	$\delta\overline{Nu}_f(\%)$
-20	09.0839	4.6642	273.8935	241.8190	11.71
-15	12.4801	4.5507	270.4404	238.8774	11.67
-10	16.8153	4.3133	265.8991	235.4435	11.45
-5	20.9749	1.6068	261.3695	241.5036	07.60
0	24.7513	3.1382	257.1503	229.1534	10.89
5	29.8328	1.7427	251.2163	229.8824	08.49
10	31.0508	3.7184	249.7750	223.1974	10.64
20	40.8977	3.2336	237.2695	213.2094	10.14
30	49.8747	2.8657	210.2988	202.1638	03.87

Table 2. Correlation coefficients of the resulting internal and external heat rates and the required cooling capacity (kW) as functions of the average temperature ($^{\circ}C$) within the nacelle : $q = \alpha\ T_{av} + \beta$

	q_{int}		q_{ext}		q_C	
	2D	3D	2D	3D	2D	3D
α	-91.69	-93.91	-2236.80	-767.52	-859.20	-2330.60
β	12199	12728	103180	41071	53270	115910